
# Electrochemical and Mechanical Effects on Charged Interfaces



| | |
|---|---|
| Journal: | *Energy & Environmental Science* |
| Manuscript ID | EE-COM-11-2017-003400.R1 |
| Article Type: | Communication |
| Date Submitted by the Author: | 23-May-2018 |
| Complete List of Authors: | Karra, Suryanarayana; Purdue University College of Education, Materials Engineering<br>Chueh, William; California Institute of Technology, Materials Science<br>Garcia , Edwin ; Purdue University, School of Materials Engineering |
| | |

Journal Name

ARTICLE TYPE

Cite this: DOI: 10.1039/xxxxxxxxxx

# Electrochemical and Mechanical Effects on Charged Interfaces†

K. S. N. Vikrant,[a] William C. Chueh,[b] and R. Edwin García,[a]

Received Date
Accepted Date

DOI: 10.1039/xxxxxxxxxx

www.rsc.org/journalname

**We establish a comprehensive space-charge treatment that includes electrochemomechanical effects to physically describe the equilibrium and transport properties of charged interfaces in ion-conducting solids. The theory is consistent with the laws of thermodynamics and Maxwell's Equations and naturally includes the free energy contributions of the chemical, electrical, and mechanical fields at and in the vicinity of homo- and heterointerfaces. In the dilute limit, and in the absence of chemomechanical stresses, the theory reduces to the classic, well-established Gouy-Chapman description. In the strong substitution limit, the model naturally predicts the appearance of a Mott-Schottky-type layer and reproduces the well known experimentally observed behavior, including grain boundary solute segregation. We demonstrate the validity of this theory for polycrystalline $Gd_yCe_{1-y}O_{2-y/2}$, GCO. In the low substitution limit, electrochemical and chemomechanically-induced stresses favor the segregation of $[Gd'_{Ce}]$ which locally expands the crystalline lattice, and thus promotes the formation of a wide depletion zone of oxygen vacancies in front of the interface, negatively impacting the macroscopic ionic conductivity. For high gadolinia substitution, interface segregation induces compressive stresses of 45 to 700MPa and a weakly tensile region in the vicinity of the GCO homointerface, as a result of coupled, long range, electrochemomechanical interactions. The accumulation of gadolinium defects at the grain boundary locks-in oxygen vacancies, which in turn suppresses the depletion zone from the extended immediate neighborhood and decreases its macroscopic ionic conductivity. This is the first model where the grain boundary core explicitly includes chemomechanical effects.**

**Broader context**

Recent theoretical and experimental studies in existing and emerging ion-conducting solids have highlighted the importance of the electrochemical and mechanical properties of grain boundaries to define the ionic transport for high performance applications, such as solid oxide fuel cells, lithium-ion batteries and super-capacitors. In all these cases, the transport properties are controlled by the defect chemistry at and near the grain boundaries, which are influenced by the associated local chemical, electrical, and mechanical stimuli. In this work, we present a thermodynamically consistent theory that incorporates the electro-chemico-mechanical effects for substitutional ionic conductors as a basis to predict the spatial defect distribution and transport properties at grain boundaries and the abutting single-crystal grains that comprise their bulk, macroscopic form. The proposed generalized theory enables the design of advanced polycrystalline ionic conductors and the identification of the microstructural transport bottlenecks by starting from experimentally measurable quantities.

Advanced ion-conducting solids are building blocks in current and emerging technologies, such as rechargeable lithium-ion batteries, solid oxide fuel cells, and gas sensors. The overall performance and reliability of these solids is dictated by their equilibrium and transport properties, and, as the world aims to develop more efficient and environmentally friendly energy storage and conversion devices, the basic understanding of the microstructural mechanisms that control and limit their response is the first step to achieve this goal[1].

Experimental studies aimed to understand the bottlenecks that control the properties in ionic conductors indicate that grain boundaries impact (favorably or unfavorably) the macroscopic charge conductivity[2–5]. Explanation of grain boundaries behavior include interfacial structural disorder[6], space-charge[7–9], segregation of impurities and dopants[2,7,10–12], and the appearance of glassy pockets[13,14]. In all these studies, it is clear that the nature of the interface also affects the properties of the abutting grains, and the overall macroscopic properties. For example, in the case of oxygen ionic conductors, such as substituted

[a] School of Materials Engineering, Purdue University, West Lafayette, Indiana 47907, United States. Tel:(765) 463-7801; E-mail: redwing@purdue.edu
[b] Material Science and Engineering, Stanford University, California 94305, United States.

$ZrO_{2-y}$ or $CeO_{2-y}$, it is well-known that the total ionic conductivity of these chemistries in its polycrystalline form is often lower due to the space charge blocking effect that develops at the grain boundary[7,15,16], and due to an excess of positively charged oxygen vacancies in the grain boundary core and an additional space charge layer of depleted oxygen vacancies in the vicinity of the interface[7,15].

Chemomechanical coupling is a well appreciated bulk effect in ionic conductors. Atomistic simulation studies on yttria stabilized zirconia interfaces under biaxial strain performed by Kushima and Yildiz shows that the ionic conductivity is enhanced due to change in the oxygen vacancy migration path that resulted from a decrease in the enthalpy of migration[17]. Chemical strain experimental studies on GCO thin films shows that stress relaxation occurs at the interface by converting mechanical energy into chemical energy, *i.e.*, changing the equilibrium defect concentration at the interface[18–20]. Recent experimental studies on $CeO_{2-y}$ strained thin films suggests that the equilibrium oxygen storage capacity is increased under both compression and tension[21]. While the experimental evidence has shed important light on the development of a fundamental understanding of the nature of homo- and heterointerfacial solids, the establishment of a thermodynamically consistent description, solely based on well-established experimentally measurable quantities that predict the formation of space charge layers and the associated thermal, structural, chemical, and mechanical responses is still missing.

In $Gd_yCe_{1-y}O_{2-y/2}$ with low Gd substitution, the total ionic conductivity is three to four orders of magnitude lower than the single crystal conductivity due to a wide depletion zone of oxygen vacancies[15,22]. In the high substitution limit, the attractive interactions between $[Gd'_{Ce}]$ and $[V_O^{\cdot\cdot}]$ induces an increase in the enthalpy of migration of oxygen defects[22,23], thus resulting in the development of a maximum in the macroscopic conductivity in the $250-500^{\circ}C$ range[15,22,24,25]. In addition, Scanlon *et al.*, showed that gadolinium accumulates at grain boundaries[26], while Lee and coworkers demonstrated through atomistic simulations the co-accumulation of oxygen vacancies and gadolinium defects at surfaces and grain boundaries[27,28]. The authors reported that the interfacial accumulation of oxygen vacancies is accompanied by a thick depletion zone of oxygen vacancies and a small depletion zone of gadolinium defects in the vicinity of the grain boundary due to space charge effects[27,28]. Finally, Zha, Xia, and Meng observed that the lattice constant increased linearly with Gd concentration, *i.e.*, follows Vegard's law[29].

Historically, Frenkel was the first to propose that space charge near the free surface in ionic conductors was a result of Schottky defects[30]. Analytical solutions describing the charged defect distribution near free surfaces, edge dislocations and grain boundaries have been formulated by several authors[31,32]. These solutions are based on the classic Poisson-Boltzmann and Gouy-Chapman approach for liquid electrolytes[8]. The Gouy-Chapman approach has been used to describe the space charge layers in the vicinity of the grain boundaries in the dilute limit. The model accounts for electrostatic segregation of defects at the interface, but does not consider the menagerie of coupled chemical, dipolar, and elastic interactions. Kliewer and Koehler were the first to introduce a variational formulation for space charge on free surfaces in ionic solids[33]. Yan, Cannon, and Bowen further extended this variational approach to describe ceramic grain boundaries to include solute segregation at interfaces due to electrostatic, dipolar, and elastic interactions[34]. The authors assumed an analytical function for the elastic energy density due to dopants in the dilute limit.

In the high substitution limit, the Mott-Schottky approximation has been used to rationalize defect distributions near interfaces. Dopants/substituents are assumed to be immobile in the vicinity of the grain boundary and typically the electrostatic potential is fitted to match the experimental observations.[7,35–38]. Sheldon and Shenoy extended the Gouy-Chapman approach and included the hydrostatic stresses induced by the accumulation of point defects[39]. The model works well for intrinsic defects. Most recently, Mabane and De Souza introduced a gradient energy penalty to tune point defect gradient in vicinity of the interface[40]. This contribution is the first to go beyond the dilute limit, but requires to fit an experimentally unmeasurable gradient energy coefficient correction[41].

Variational and phase field formulations that resolve the effect of charge and polarization in ionic conductors include those proposed by Chen and Khachaturyan[42]. Later, Bishop, García, and Carter developed a variational formulation to study charged domains in a spinodally decomposing (phase separating) ionic solid[43]. García, and coworkers generalized these ideas into a theoretical framework to describe the local equilibrium and phase transformation kinetics of electrically active ionic solids[44], and provided the basis to naturally incorporate Maxwell's Equations to develop thermodynamically consistent phase field formulations. Guyer *et al.*, developed independently a conceptually equivalent diffuse interface model to capture the effects of charge separation associated with the equilibrium double layer at an electrochemical interface[45].

The Langmuir-McLean theoretical model[46,47], predicts the segregation of point defects in the absence of electrostatic, dipolar and elastic interactions. Li, Obiani, and Darken were the first to include elastic interactions to describe the segregation of dopants at grain boundaries[48]. The model describes crystallographically isotropic solids in the dilute limit. Several authors,[26–28], have followed up on these ideas and have readily demonstrated that acceptor-doped oxides chemically expand the crystalline lattice and induce stresses in the vicinity of grain boundaries.

In this paper, a thermodynamically consistent variational theory is proposed to naturally include the effects of non-diluted segregation, dipolar and self-induced electric field effects, as well as long range, chemically induced (chemomechanical) elastic energy density contributions to the total free energy of the system. The developed model provides a rational basis to understand the stability of point defect distributions away from the interface and its effect on the charge transport properties of the corresponding polycrystalline chemistries. The theory is demonstrated on GCO and validated against experimentally measured properties.

Define the Helmholtz free energy per unit volume, $f$, for an ionic conductor as a function of $N$ charged species, including

point defects, $[V_1^{Z_1}],\ldots,[V_N^{Z_N}]$, as classically defined[49], and define $\eta$ as a coarse-grained measure of the crystallinity (atomic ordering) in the ionic ceramic phase, so that $\eta = 1$ corresponds to a perfectly crystalline lattice and $\eta = 0$ to a disordered region[50] (See Supplemental Information for Table of symbols Summary). Each component has associated a formal valence $Z_N$, which in turn contributes to increase the electrostatic energy, $\rho\phi$, and an additional contribution to the density of dipole moments, $\frac{1}{2}\vec{D}\cdot\vec{E}$, to the system, $f_\circ$, in agreement with Hart[51], and García *et al.*[44]:

$$\begin{aligned} f_\circ(\eta,[V_1^{Z_1}],\ldots,[V_N^{Z_N}],\rho,\vec{D};T) &= f([V_1^{Z_1}],\ldots,[V_N^{Z_N}];T) \\ &\quad +\rho\phi+\tfrac{1}{2}\vec{D}\cdot\vec{E} \end{aligned} \tag{1}$$

The spatial distribution of electrostatic charge raises the free energy of the system, $f_\circ$, when the local charge density, $\rho$, has the same sign as the electrostatic potential, $\phi$, while the second, dipolar term penalizes the increase of electrostatic energy that may result from the formation of local charge inhomogeneities.

The electrochemical free energy density, $f_{ec}$, of the system is defined through the Legendre transformation[44,49,52], $f_{ec}(\eta,[V_1^{Z_1}],\ldots,[V_N^{Z_N}],\vec{E};T) = f_\circ(\eta,[V_1^{Z_1}],\ldots,[V_N^{Z_N}],\vec{D};T) - \vec{D}\cdot\vec{E}$ which specifies that the free energy per unit volume decreases when the material is electrostatically polarized, in agreement with several authors[43–45]. In addition, the electrostatic potential, $\phi$, and the electric field, $\vec{E}$, are related through the relation, $\vec{E} = -\nabla\phi$, because the position-dependent electric field is a solution of Faraday's Law, $\nabla\times\vec{E} = \vec{0}$, for a constant magnetic induction field. Finally, the total polarization and the electric field are related through the well-known constitutive equation, $\vec{D} = \epsilon\vec{E} = -\epsilon\nabla\phi$, in the absence of piezoelectric and pyroelectric effects.

In agreement with Larché and Cahn[53], each chemical species imposes a change in the lattice parameter of the local crystal structure, which in turn results on the development of elastic stresses. Mathematically, this is specified by the modified Hooke's law[54]:

$$\sigma_{ij} = C_{ijkl}\left(\varepsilon_{kl} - \sum_{m=1}^{N}\beta_{kl}^{(m)}([V_m^{Z_m}]-[V_m^{Z_m}]_\circ)\right) \tag{2}$$

In the small deformation limit, the mechanical displacement, $\vec{u} = (u_1,u_2,u_3)^T$, and the geometrical strain, $\varepsilon_{ij}$, are related through the expression:

$$\varepsilon_{ij} = \frac{1}{2}\left(\frac{\partial u_i}{\partial x_j}+\frac{\partial u_j}{\partial x_i}\right) \tag{3}$$

Thus, the development of ionic defect-induced lattice parameter changes will result in elastic energy inhomogeneities, *i.e.*, $\frac{1}{2}\overleftrightarrow{\sigma}\cdot\overleftrightarrow{\varepsilon}_e \geq 0$, which in turn will contribute to the free energy functional[44]:

$$\begin{aligned} F[\eta,[V_1^{Z_1}],\ldots,[V_N^{Z_N}],\phi,u_1,u_2,u_3;T] &= \int_V \Big[f(\eta,[V_1^{Z_1}],\ldots,[V_N^{Z_N}],T) \\ &\quad +\rho\phi-\tfrac{\epsilon}{2}(\nabla\phi)^2 \\ &\quad +\tfrac{1}{2}\overleftrightarrow{\sigma}\cdot\overleftrightarrow{\varepsilon}_e\Big]d\Omega \end{aligned} \tag{4}$$

For ease in the description, phase separation in the Gibbsian sense[52], including spinodal decomposition effects, as described by Cahn and Hilliard[41], are not included; however, they can be easily incorporated, *e.g.*, see[43,55]. In general, the chemical expansion of the lattice parameter is a function of composition as has been reported in the scientific literature, *e.g.*,[56]. For simplicity, non-linearity in chemical expansion is not considered in this work, though it can be easily incorporated. The local charge density is coupled to the spatial distribution of the different chemical species through the expression, $\rho = \sum_{i=1}^{N} eZ_i[V_i^{Z_i}]$, in agreement with Bishop[43], Guyer *et al.*[45], and generalizations by García *et al.*[44]. Finally, the chemical free energy density of an ionic solution, $f$, possesses contributions to the free energy of formation, $f_i(\eta,T)$, and entropic and the enthalpic free energies of mixing, of the dissolved chemical species and phases through the expression:

$$\begin{aligned} f(\eta,[V_1^{Z_1}],\ldots,[V_N^{Z_N}],T) &= \tfrac{1}{v}\Big(\textstyle\sum_{i=1}^{N}(f_i(\eta,T)[V_i^{Z_i}]+k_bT[V_i^{Z_i}]\ln[V_i^{Z_i}]) \\ &\quad +k_bT(1-\textstyle\sum_{i=1}^{N}[V_i^{Z_i}])\ln[1-\textstyle\sum_{i=1}^{N}V_i^{Z_i}] \\ &\quad +\textstyle\sum_{j=1,i\neq j}^{N}\Omega_{ij}[V_i^{Z_i}][V_j^{Z_j}]\Big) \end{aligned} \tag{5}$$

where $f_i(\eta,T) = f_i^X(T)p(\eta)+f_i^S(T)(1-p(\eta))$. Here, spatial inhomogeneities on the structural disorder, such as those occurring at the grain boundary, will energetically favor the attraction of those ionic species and point defects whose energy of formation is lower than those displayed in structurally ordered regions, in agreement with classic phase field formulations[50].

Equation 4 leads to a set of local equilibrium conditions, represented by the variational derivatives:

$$\begin{aligned} \tfrac{\delta F}{\delta\phi} &= \nabla\cdot\epsilon\nabla\phi+\rho = 0 \\ \tfrac{\delta F}{\delta u_i} &= \nabla\cdot\overleftrightarrow{\sigma} = 0 \\ \tfrac{\delta F}{\delta[V_i^{Z_i}]} &= \xi_i = \tfrac{\partial f}{\partial[V_i^{Z_i}]}+Z_ie\phi-\overleftrightarrow{\sigma}\cdot\overleftrightarrow{\beta}^{(i)} \end{aligned} \tag{6}$$

The first row of Equation 6 corresponds to Coulomb's equation, in agreement with the classical electromagnetics literature[57], and previous work[43–45]. The second row of Equation 6 corresponds to the mechanical equilibrium equation, in agreement with continuum mechanics theory[58], and previous work[44]. Finally, the third row of Equation 6 is identified as the electrochemomechanical potential of the *i*th ionic species, $\xi_i$, and reduces to the well-known electrochemical potential in the absence of local stresses[43–45], and to the chemical potential in the absence of stresses and electrostatic charge. The electrochemicomechanical potential defines a generalized intensive local thermodynamic driving force for mass (and charge) segregation at interfaces as a result of gradients of chemical potential, electrostatic potential, or stresses. Overall, the electrical, mechanical, and chemical state of a grain boundary and the surroundings are determined by simultaneously solving the set of equations, as determined by Equation 6.

For a grain boundary in local thermodynamic equilibrium with the surrounding abutting grains[53], the electrochemomechanical potential of the grain boundary core, $S$, and the volume of the crystalline solid, $X$, are equal and spatially uniform, *i.e.*, $\xi_i^S = \xi_i^X$, which results into the concentration distribution for each of the *i*th species, $[V_i^{Z_i}]$:

$$\frac{\frac{[V_i^{Z_i}]}{1-\sum_{i=1}^{N}[V_i^{Z_i}]}}{\frac{[V_i^{Z_i}]_S}{1-\sum_{i=1}^{N}[V_i^{Z_i}]_S}} = \exp\left[\frac{-((1-p(\eta_\circ)\Delta f_{V_i^{Z_i}}^{S\to X}) + \sum_{j=1,i\neq j}^{N}\Omega_{ij}([V_j^{Z_j}]-[V_j^{Z_j}]_S) + Z_i e(\phi-\phi_\circ) - (\overleftrightarrow{\sigma}\cdot\overleftrightarrow{\beta}^{(i)} - (\overleftrightarrow{\sigma}\cdot\overleftrightarrow{\beta}^{(i)})_S))}{k_bT}\right] \quad (7)$$

Equation 7 reduces to the classical Gouy-Chapman description, $[V_i^{Z_i}] = [V_i^{Z_i}]_\infty \exp(-Z_i e\phi/k_bT)$, in the limit of an ideal, dilute, solution, in the absence of elastic stresses. Away from this limit, the degree of crystallographic disorder at the interface provides a natural driving force for grain boundary solute accumulation and specifies the maximum number of accessible segregation sites. In the absence of charge, Equation 7 reduces to the Langmuir-McLean equation, *i.e.*, $\frac{[V_i^{Z_i}]_S}{1-[V_i^{Z_i}]_S} = \frac{[V_i^{Z_i}]_\infty}{1-[V_i^{Z_i}]_\infty}\exp[\frac{\Delta f^{S\to X}}{k_bT}]$,[46,47].

While the spatial extent of a charged layer (*i.e.*, a generalized Debye length) is a direct function of the bulk composition, Equation 7 shows that because mechanical stresses in the crystalline solid are capable of extending across large distances away from its source, stress inhomogeneities will have a very strong, nontrivial influence on the spatial extent of the segregant. In addition, interfacial stresses will shift the electrostatic potential, further disturbing the interface segregation extent, and thus the spatial distribution of the defects. Also, the chemical stress differences between the interface and the abutting grains, induced by the differences in Vegard strain between the interface and surrounding crystalline solid, will have an influence on the solute distribution and are capable of inducing ionic segregation at distances that go well beyond the structural location of the interface. Finally, Equation 7 readily demonstrates that stress gradients increase the extent of the charge layer, and its width is proportional to the elastic stiffness of the crystalline phase.

**Table 1** Summary of physical parameters used in the interface defect distribution calculation (See Supplemental Information for Table of symbols Summary).

| Symbol | Value(units) | Ref. |
|---|---|---|
| $Z_O$ | 2 | – |
| $Z_{Gd}$ | $-1$ | – |
| $f_{V_O^{\cdot\cdot}}^S - f_{V_O^{\cdot\cdot}}^X$ | $-2.0$ eV | 59 |
| $f_{Gd'_{Ce}}^S - f_{Gd'_{Ce}}^X$ | 0.0 eV | 40 |
| $\Omega_{Gd'_{Ce}V_O^{\cdot\cdot}}$ | $-0.3$ eV | 22 |
| $\nu_\circ$ | $4\times10^{-29}$ m$^3$/atom | – |
| $\delta$ | 2 nm | – |
| $\eta_\circ$ | 0 | – |
| $\epsilon_r$ | 35 | 60 |
| $\beta_T$ | 0.00095 | 29 |
| $E$ | 190 GPa | 61 |
| $\nu$ | 0.3 | 61 |

This formulation was applied to describe the properties of polycrystalline GCO. Properties are summarized in Table 1 (See Supplemental Information for more details), as experimentally reported by[22,29,59–61]. Except for the mechanical[61] and chemomechanical properties[29], used values are the same as those used by[40]. Consistent with phase field formulations, our solution domain spans both the grain boundary core, space-charge region, and the bulk. For simplicity, we assume that the grain boundary core has the same mechanical properties and $[V_O^{\cdot\cdot}]$ ionic mobility as the bulk. Also, the dependence of $[V_O^{\cdot\cdot}]$ ionic mobility on strain was not included. Finally, the chemical expansion is taken to be linear and assumed to be dominated by $[Gd'_{Ce}]$. In other words, $[V_O^{\cdot\cdot}]$ is assumed to be zero Vegard constant. We made this approximation because it is not possible to experimentally determine the Vegard constants for these two defects separately as they are coupled by electroneutrality in the bulk. Nevertheless, we carried out a sensitivity analysis on the Vegard constants of $[Gd'_{Ce}]$ and $[V_O^{\cdot\cdot}]$ (see Supplemental Information). We show that this assumption does not affect the transport behavior of GCO at low substitution levels, since the grain boundary core width is much smaller than the space-charge width.

The predicted spatial distribution of $[V_O^{\cdot\cdot}]$ and $[Gd'_{Ce}]$ in the vicinity of the grain boundary is shown in Figure 1 (a), for $Gd_yCe_{1-y}O_{2-y/2}$ at $T = 1300^\circ$C and $y = 0.01$. The grain boundary core is $[V_O^{\cdot\cdot}]$-rich, in agreement with experimental results[7,15,24,29]. Also, the accumulation of $[V_O^{\cdot\cdot}]$ very close to the interface draws point defects from the immediate surroundings and results in the formation of a depletion zone of oxygen vacancies two nanometers away from the interface. Accumulation of $[Gd'_{Ce}]$ in the grain boundary core is a result of the interfacial oxygen vacancy pile up, $f_{V_O^{\cdot\cdot}}^S - f_{V_O^{\cdot\cdot}}^X = -2.0$eV, which attracts point defects of opposite polarity. The calculation demonstrates that the induced concentration gradients favor compressive stresses at the center of the grain boundary core, which in turn promotes the formation of a wide elastic energy region some distance away from the interface (see Figure 1 (b)). The increase of the local free energy of the system due to the chemomechanical coupling discourages the appearance of sharp concentration gradients of $[Gd'_{Ce}]$ and $[V_O^{\cdot\cdot}]$, increasing the extent of the depletion/accumulation zone from 10 to $\sim$17nm, defined herein as the distance away from the interface where the system deviates from charge neutrality by 1%, in agreement with the experimental observations in YSZ[11]. Interestingly, inclusion of chemomechanical effects increases the charge density at the grain boundary core (see Figure 1 (c)), because compressive stresses disfavor the accumulation of negatively charged $[Gd'_{Ce}]$ in the grain boundary core. Overall, the calculation demonstrates that in order to minimize the combined electrochemical and chemomechanical contributions to the free energy of the system, the segregated and depleted ionic species have to increase their spatial extent while simultaneously forcing the elastic stress at the interface to decrease to a minimal value. The resultant plane-stress distribution in the vicinity of the interface reaches a compressive extreme value $\sim$2nm in front of the interface as a result of the Vegard strain contribution from Gd, and it becomes stress free $\sim$20nm away from the boundary.

The effect of substitution on the point defect distribution is shown in Figure 2. Results demonstrate that as the macroscopic

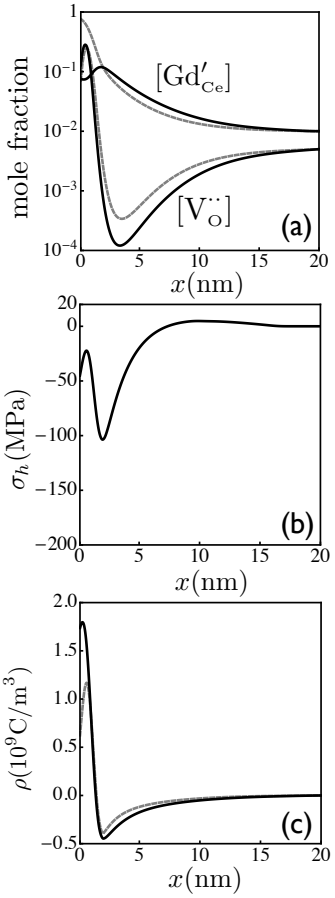


**Fig. 1** Predicted defect concentration (inset (a)), hydrostatic stress (inset (b)), and charge density (inset (c)) in the vicinity of grain boundary for $Gd_yCe_{1-y}O_{2-y/2}$, for $y = 0.01$. $[Gd'_{Ce}]$ segregate at the interface ($x = 0$ nm) due to the development of a positive interfacial potential. The accumulated gadolinium defects at the interface expands the ceria lattice and imposes a compressive hydrostatic stress. The developed stress decreases the gadolinium defect concentration, which, in turn, increases the spatial extent of the oxygen vacancies. As a point of comparison, the predicted defect concentration and charge density distributions without chemomechanical couplings are shown as dash gray lines.

concentration of gadolinia increases, the spatial extent of segregation decreases from 17 to ∼4nm. At low substitution levels, the $[Gd'_{Ce}]$ peaks at ∼2nm from the center of the grain boundary core. At high substitution levels, it peaks at the center of the grain boundary core. This $[Gd'_{Ce}]$ segregation reflects electrostatic, mechanical, and defect-defect interaction contributions, as we did not consider a segregation energy for $[Gd'_{Ce}]$. A shallow depletion region of $[Gd'_{Ce}]$ is also favored ∼2nm away from the interface for higher substitution levels, and has a thickness of ∼0.5nm. The substituent depletion region shifts away from the interface due to increase in the thickness of segregation region of substituent. Also, the grain boundary core accumulation of $[V^{\cdot\cdot}_O]$ increases by a factor of two, while the oxygen vacancies depletion region significantly decreases from a two orders of magnitude difference to an experimentally negligible amount. The charge point defect redistribution associated with gadolinia induces a very large compressive stress in the grain boundary core because of the large lattice expansion induced by the accumulation of $[Gd'_{Ce}]$. To enforce mechanical equilibrium from the lattice expansion driven by the addition of $[Gd'_{Ce}]$, a tensile region forms in the vicinity of the oxygen vacancy depletion region. The enrichment factor, *i.e.*, the ratio of substituent concentration at the grain boundary core to average substituent concentration is 4.45 for $y = 0.2$, in very good agreement with the reported experimental value of 4.2[26]. Overall, calculations demonstrate that for large amounts of substitution, $[Gd'_{Ce}]$ accumulates uniformly at the grain boundary for a thickness of ∼1.5nm in agreement with atomistic calculations[28], leading to a spatial distribution of point defects that correspond to a stress induced Mott-Schottky type interface[35,62].

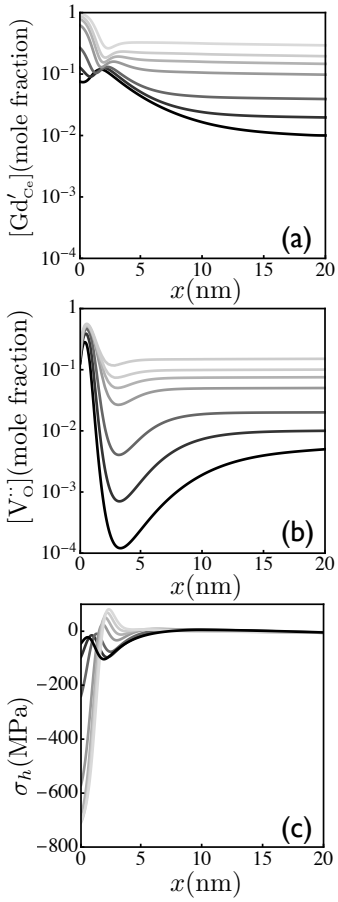


**Fig. 2** Effect of gadolinia substitution on the spatial distribution of point defects. Inset (a) shows $[Gd'_{Ce}]$ distribution, (b) shows $[V^{\cdot\cdot}_O]$ distribution, and (c) shows hydrostatic stress distribution. The shade of gray changes from dark to light with $Gd_yCe_{1-y}O_{2-y/2}$ substituent $y = 0.01$ (darkest), $y = 0.02$, $y = 0.04$, $y = 0.1$, $y = 0.15$, $y = 0.20$, and $y = 0.30$ (lightest).

Figure 3 summarizes the effect of substituent on the electrostatic interfacial potential. In the $0.01 < y < 0.1$ range, the electrostatic potential increases by 150mV as a result of the increase in $[V^{\cdot\cdot}_O]$ accumulation at the interface. In the high substitution limit, $0.1 < y < 0.3$, the interfacial accumulation of $[V^{\cdot\cdot}_O]$ and $[Gd'_{Ce}]$ defects contribute to an additional increase of the electrostatic potential by 50mV. Calculations show that the electrostatic potential increases with substituent concentration because the driving force to accumulate oxygen vacancies at the grain boundary

core increases the electrochemicomechanical potential. This favors the formation of larger electrostatic potentials and promotes the chemical attraction of $[V_O^{\cdot\cdot}]$ and $[Gd'_{Ce}]$, while decreasing the extent of the electrostatic potential distribution, from 17nm to 4nm. Further, as the amount of gadolinia increases in the grain boundary, the developing Vegard stresses enhance the interfacial electrostatic core potential by a few milivolts with respect to the stress-free system. This effect becomes apparent at high substitution levels, and demonstrates that while the grain boundary has a strong influence on the surrounding grains, these also affect the electrochemomechanical state of the interface.

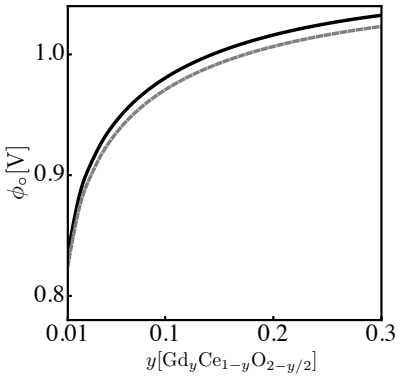


**Fig. 3** Predicted interfacial electrostatic potential as a function of $Gd_yCe_{1-y}O_{2-y/2}$ for only electrostatic and chemical driving forces (gray dashed line) and with full electrostatic, chemical and mechanical driving forces (black solid line).

Figure 4 summarizes the predicted and experimental effect of gadolinia on the macroscopic conductivity of polycrystalline $Gd_yCe_{1-y}O_{2-y/2}$, for grain sizes larger than 500nm. Experimental data corresponds to samples quenched from 1300°C and measured at 440°C, as reported by Tschöpe and coworkers [15]. A direct comparison shows an excellent agreement. In the absence of chemicomechanical stresses, the calculated conductivity is two orders of magnitude larger than experimentally observed values, particularly in the small substitution regime, $0.01 < y < 0.1$. In contrast, the incorporation of elastic energy contributions and chemomechanical couplings extends the oxygen vacancy depletion zone beyond the width of the grain boundary and significantly contributes to decrease the macroscopic ionic conductivity. In the intermediate substitution regime, $0.1 < y < 0.15$, the oxygen vacancies depletion zone disappears, and results in an increase in the total conductivity, so that a maximum for polycrystalline $Gd_yCe_{1-y}O_{2-y/2}$, occurs at $y = 0.15$ in very good agreement with experimental results [15]. Finally, in the high substitution limit, $0.1 < y < 0.3$, the electrochemical defect interactions between oxygen vacancies and substituents decrease the ionic mobility of oxygen vacancies and leads to a decrease in the total conductivity.

## Conclusions

In conclusion, a thermodynamically consistent space charge theory was developed, in excellent agreement with well-established experimental results. The local interfacial behavior is a direct consequence of the electrostatic, chemical, and chemomechanical driving forces that attempt to minimize the total free energy of the system as a result of the underlying, segregation-induced chemical stresses. Conceptually, the model predicts a substituent concentration distribution function reminiscent of the Mott-Schottky approximation, with a direct and converse chemomechanical coupling, which naturally redistributes the charged species and stretches the extent of the electrochemical interface, as demonstrated for GCO. Further, for the generality of ionic conductors, the developed theory provides the ideal basis to understand the transport limitations for ceramic systems for a wide variety of energy-related applications, including electrolytes for solid oxide fuel cells, electrode chemistries for currently used Li-ion batteries, and solid electrolytes for emerging solid state batteries.

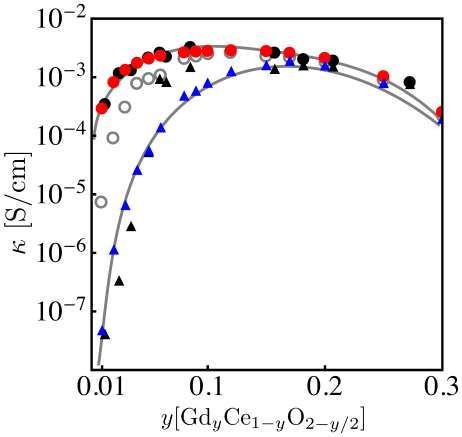


**Fig. 4** Experimental and simulated ionic conductivity for $Gd_yCe_{1-y}O_{2-y/2}$. Experimental single-crystal ionic conductivity corresponds to ● and experimental polycrystalline conductivity corresponds to ▲, [15]. Samples were quenched from 1300°C and measured at 440°C. Simulated single-crystal ionic conductivity corresponds to ●, calculated polycrystalline ionic conductivity only including electrostatic and chemical driving forces corresponds to ○, and including all the chemical, electrostatic, and mechanical driving forces, corresponds to ▲. Gray lines are a guide to the eye.

## Acknowledgments

KSNV and REG thank the support provided by US ONR N00014-17-1-2087. WCC and REG acknowledge support from Toyota Research Institute through the D3BATT Center for Data-Driven Design of Lithium-Ion Batteries.

## Conflict of interest

There are no conflicts of interest to declare.

## References

1 B. V. Lotsch and J. Maier, *J. Electro. Ceram.*, 2017.
2 L. Malavasi, C. A. J. Fisher and M. S. Islam, *Chem. Soc. Rev.*, 2010, **39**, 4370–4387.
3 J. Maier, *Phys. Chem. Solid.*, 1985, **46**, 309–320.
4 X. Guo and R. Waser, *Progress in Materials Science*, 2006, **51**, 151–210.
5 S. Ramanathan, *J. Vac. Sci. Technol. A*, 2009, **27**, 1126–1134.
6 A. Kayyar, H. J. Qian and J. Luo, *Appl. Phys. Lett.*, 2009, **95**, 221905.
7 X. Guo, W. Sigle and J. Maier, *J. Am. Ceram. Soc.*, 2003, **86**, 77–87.
8 J. Maier, *Prog. Solid. State.*, 1995, **23**, 171–263.
9 M. Vollman and R. Waser, *J. Am. Ceram. Soc.*, 1994, **77**, 235–243.
10 M. Aoki, Y.-M. Chiang, I. Kosacki, L. Lee and H. T. Y. Liu, *J. Am. Ceram. Soc.*, 1996, **79**, 1169–1180.

11 N. Shibata, Y. Ikuhara, F. Oba, T. Yamamoto and T. Sakuma, *Philos. Mag. Lett.*, 2002, **82**, 393–400.
12 Y. Ikuhara, P.Thavorniti and T. Sakuma, *Acta Mater.*, 1997, **45**, 5275–5284.
13 B. Kang and G. Ceder, *Nature*, 2009, **458**, 190–193.
14 J. Luo, *Crit. Rev. Solid. State. Mater. Sci.*, 2007, **32**, 67–109.
15 A. Tschöpe, S. Kilassonia and R. Birringer, *Solid State Ionics*, 2004, **173**, 57–61.
16 X. Guo, *Solid State Ionics*, 1995, **81**, 235–242.
17 A. Kushima and B. Yildiz, *J. Mater. Chem.*, 2010, **20**, 4809–4819.
18 M. Greenberg, E. Wachtel, I. Lubomirsky, J. Fleig and J. Maier, *Adv. Funct. Mater.*, 2006, **16**, 48–52.
19 A. Kossoy, Y. Feldman, E. Wachtel, I. Lubomirsky and J. Maier, *Adv. Funct. Mater.*, 2007, **17**, 2393–2398.
20 K. Song, H. Schmid, E. G. V. Srot, G. Gregori, K. Du, J. Maier and P. A. V. Aken, *APL Materials*, 2014, **2**, 032104.
21 C. B. Gopal, M. G. Melchor, S. C. Lee, Y. Shi, A. Shavorskiy, M. Monti, Z. Guan, R. Sinclair, H. Bluhm, A. Vojvodic and W. C. Chueh, *Nat. Comms.*, 2017, **8:15360**, 1–12.
22 S. Grieshammer, B. O. H. Grope, J. Koettgen and M. Martin, *Phys. Chem. Chem. Phys.*, 2014, **16**, 9974–9986.
23 D. E. P. Vanpoucke, P. Bultinck, S. Cottenier, V. V. Speybroeck and I. V. Driessche, *J. Mater. Chem. A*, 2014, **2**, 13723–13737.
24 T. S. Zhang, J. Ma, H. Cheng and S. H. Chan, *Materials Research Bulletin*, 2006, **41**, 563–568.
25 B. C. H. Steele, *Solid State Ionics*, 2000, **129**, 95–110.
26 P. J. Scanlon, R. A. M. Bink, F. P. F. V. Berkel, G. M. Christie, L. J. V. Ijzendoorn, H. H. Brongersma and R. G. V. Welzenis, *Solid State Ionics*, 1998, **112**, 123–130.
27 H. B. Lee, F. B. Prinz and W. Cai, *Acta Materialia*, 2010, **58**, 2197–2206.
28 H. B. Lee, F. B. Prinz and W. Cai, *Acta Materialia*, 2013, **61**, 3872–3887.
29 S. Zha, C. Xia and G. Meng, *J. Pow. Sou.*, 2003, **115**, 44–48.
30 J. Frenkel, *Kinetic Theory of Liquids*, Oxford University Press, New York, 36th edn, 1946.
31 K. Lehovec, *J. Chem. Phys.*, 1953, **21**, 1123.
32 J. D. Eshelby, C. W. A. Newey, P. L. Pratt and A. B. Lidiard, *Phil. Mag.*, 1958, **3**, 75–89.
33 K. L. Kliewer and J. S. Koehler, *Phys. Rev.*, 1965, **140**, A1226–A1240.
34 M. F. Yan, R. M. Cannon and H. K. Bowen, *J. Appl. Phys.*, 1983, **54**, 764.
35 J. Luo, *J. Materiomics*, 2015, **1**, 22–32.
36 N. F. Mott, *Proc. Roy. Soc. (London) A.*, 1939, **171**, 27.
37 W. Z. Schottky, *Physik*, 1939, **113**, 367.
38 S. Kim and J. Maier, *J. Elec. Soc.*, 2002, **149**, J73–J83.
39 B. W. Sheldon and V. B. Shenoy, *Phys. Rev. Lett.*, 2011, **106**, 216104.
40 D. S. Mebane and R. A. D. Souza, *Energy & Environmental Science*, 2015, **8**, 2935.
41 J. W. Cahn and J. E. Hilliard, *J. Chem. Phys.*, 1958, **28**, 258–267.
42 L. Q. Chen and A. G. Khachaturyan, *Phys. Rev. Lett.*, 1993, **70**, 1477–1480.
43 C. M. Bishop, R. E. García and W. C. Carter, *Acta Mater.*, 2003, **51**, 1517–1524.
44 R. E. García, C. M. Bishop and W. C. Carter, *Acta Mater.*, 2004, **52**, 11–21.
45 J. E. Guyer, W. J. Boettinger, J. A. Warren and G. B. McFadden, *Phys. Rev. E.*, 2004, **69**, 021603.
46 D. McLean, *Grain Boundaries in Metals*, Oxford, Clarendon Press, 1st edn, 1957.
47 S. Hofmann, *J. de chimie physique*, 1992, **84**, 141–147.
48 J. C. M. Li, R. A. Oriani and L. S. Darken, *Physilkalische Chemic Neue Folge Bd*, 1966, **49**, 271–290.
49 R. T. DeHoff, *Thermodynamics in Materials Science*, McGraw-Hill, New York, 2nd edn, 1993.
50 R. Kobayashi, J. A. Warren and W. C. Carter, *Physica D*, 2000, **140**, 141–150.
51 E. W. Hart, *Phys.Rev.*, 1959, **113**, 412–416.
52 J. W. Gibbs, *Phys.Rev.*, 1878, **44**, 108–437.
53 F. Larche and J. W. Cahn, *Acta Metalurgica*, 1973, **21**, 1051–1063.
54 J. F. Nye, *Physical Properties of Crystals. Their Representation by Tensors and Matrices*, Oxford University Press, London, 1998.
55 M. Tang, W. C. Carter and R. M. Cannon, *Phys. Rev. Lett.*, 2006, **97**, 075502.
56 J. G. Swallow, W. H. Woodford, Y. Chen, Q. Lu, J. J. Kim, D. Chen, Y.-M. Chiang, W. C. Carter, B. Yildiz, H. L. Tuller and K. J. V. Vliet, *J. Electroceramics*, 2014, **32**, 3–27.
57 J. D. Jackson, *Classical Electrodynamics*, Wiley, New York, 1975.
58 S. Suresh, *Fatigue of Materials*, Cambridge University Press, Cambridge, United Kingdom, 1998.
59 Y.-M. Chiang, E. B. Lavik and D. A. Blom, *NanoStructured Materials*, 1997, **9**, 633–642.
60 D. P. Thompson and A. M. Dickins, *J. Mater. Sci.*, 1992, **27**, 2267–2271.
61 K. Yasuda, K. Uemura and T. Shiota, *Journal of physics:Conference series*, 2012, **339**, 012006.
62 X. Guo and R. Waser, *Solid State Ionics*, 2004, **173**, 63–67.